

An SPDE Based Spatio-temporal Model for Large Data Sets with an Application to Postprocessing Precipitation Forecasts

Fabio Sigrist, Hans R. Künsch, Werner A. Stahel
Seminar for Statistics, Department of Mathematics, ETH Zürich
8092 Zürich, Switzerland

April 25, 2022

Abstract

Increasingly larger data sets of processes varying in space and time are obtained in many areas. Hence, there is a growing need for statistical models and methods that can deal with such data.

We introduce a dynamic spatio-temporal model for large data sets. The solution of a stochastic partial differential equation (SPDE) is approximated in the spectral space. To cope with high spatial and temporal resolution, dimension reduction is obtained by considering a small number of Fourier basis functions. This leads to a physically motivated parametrization of a spatio-temporal Gaussian process having a nonseparable and, potentially, temporally nonstationary covariance structure. The SPDE explicitly models phenomena such as transport and diffusion that occur in many natural processes in diverse fields ranging from environmental sciences to ecology.

The incorporation of forecasts from a numerical weather prediction (NWP) model in a statistical model is generally called postprocessing. It provides calibrated and probabilistic forecasts. The proposed model is applied to postprocessing of precipitation forecasts for northern Switzerland. The postprocessed forecasts outperform the raw NWP predictions and they quantify prediction uncertainty.

KEYWORDS: space-time model, large data sets, physics based model, advection-diffusion equation, hierarchical Bayesian model, numerical weather prediction

1 Introduction

Increasingly larger spatial and spatio-temporal data sets are obtained, for instance, from remote sensing satellites or deterministic physical models such as numerical weather prediction (NWP) models. They ask for statistical models that can cope with such data. Traditional geostatistical models run into computational bottlenecks with high dimensional data since the computational cost to factorize dense $N \times N$ covariance matrices is $O(N^3)$. Banerjee et al. (2004) refer to this as the “big N problem”. In the case of spatio-temporal data, this problem is further aggravated since then one basically has $NT \times NT$ covariance matrices, N and T being the number of points in space and time, respectively.

For purely spatial data, there are two principal ways to alleviate this computational burden: reduced rank approximations and sparse matrix approximations. In the first case, covariance matrices having a reduced rank are used, and computational cost then depend on this rank rather than on the number of points in space. Typically, the dimension is reduced by using a small set of basis functions. Predictive processes (Banerjee et al. 2008) and fixed rank kriging (Cressie and Johannesson 2008) are two known examples. Nychka et al. (2002) use wavelets with varying resolutions as basis functions. Stein (2008) uses a low rank covariance matrix capturing large scale variation and adds a term with fine scale spatial structure to it. The second approach relies on the fact that calculations for sparse matrices can be done efficiently. For instance, the cost for factorizing sparse covariance or precision matrices of two-dimensional Gaussian fields is $O(N^{3/2})$ instead of $O(N^3)$ for dense matrices. Gaussian Markov random-fields (GMRF) (Rue and Tjelmeland 2002; Rue and Held 2005) have sparse precision matrices and thus can decrease computational cost. Recently, using finite element approximations to stochastic partial differential equations, Lindgren et al. (2011) show how to approximate continuously indexed Gaussian fields with GMRFs. On the other hand, Furrer et al. (2006) apply tapering to obtain sparse covariance matrices. Another proposed solution to reduce the computational burden is to approximate the likelihood so that it can be evaluated faster (Vecchia 1988; Stein et al. 2004; Fuentes 2007; Eidsvik et al. 2011).

There are two basic paradigms for constructing spatio-temporal models. The first approach is descriptive and follows the traditional geostatistical paradigm, using joint space-time covariance functions (Jones and Zhang 1997; Cressie and Huang 1999; Gneiting 2002; Ma 2003; Stein 2005; Paciorek and Schervish 2006). The second approach is dynamic and combines ideas from time-series and spatial statistics methods (Solna and Switzer 1996; Wikle and Cressie 1999; Huang and Hsu 2004; Xu et al. 2005; Gelfand et al. 2005; Johannesson et al. 2007; Sigrist et al. 2012). Whereas the former approach typically ignores the fundamental distinction between time and space, the latter uses the natural ordering of time and can be physically motivated. Besides lack of realism, the descriptive approach specifying a joint space and time covariance matrix suffers even more from the “big N problem” than the dynamic one, which can reduce computational cost due to the temporal Markov property. Concerning the construction of dynamic spatio-temporal models, Wikle and Hooten (2010) suggest to use

a priori scientific process information to motivate realistic parametrizations. They acknowledge that this idea is not new in the statistical science. For instance, Hotelling (1927) states that “indeed the use of differential equations supplies the statistician with a powerful tool, replacing the purely empirical fitting of arbitrary curves by a reasonable resultant of general considerations with particular data.”

In the following, a dynamic spatio-temporal model for spatially and temporally highly resolved data is presented. The model is based on a physically realistic process that is defined through an SPDE. Dimension reduction is obtained by approximating the solution of the SPDE in the spectral space with a low rank approximation in space. In doing so, the goal is not to approximate the exact solution as well as possible but rather to obtain a realistic parametrization of a space-time covariance structure that allows for handling large data sets. As Sun et al. (2012) state, when dealing with large data problems, one has to “sacrifice some unimportant information”. We include only lower spatial frequencies in the dimension reduced spatio-temporal model. The error introduced by ignoring the higher frequencies is then compensated by adding a term that captures small scale spatial variation and has no temporal structure. Fourier functions have several advantageous properties. First, they form an orthonormal basis. Further, they are eigen functions of the differential operator used in the SPDE meaning that differentiation in the physical space corresponds to multiplication in the spectral space. In addition, the fast Fourier transform (FFT) can be used for efficiently computing the transform from the spectral space to the physical space, and vice versa.

The remainder of this paper is organized as follows. Section 2 introduces the continuous space-time model defined through an SPDE. In Section 3, we show how to obtain a low rank approximation that can handle large spatio-temporal data sets. Next, in Section 4, it is shown how to use the spatio-temporal model as part of a hierarchical Bayesian model for modeling precipitation. After showing how to fit the model to data in Section 5, we then apply this model to postprocessing of precipitation forecasts in Section 6.

2 A Continuous Space-Time Model

In one dimension, a fundamental process is the Ornstein-Uhlenbeck process, which is governed by a relatively simple stochastic differential equation (SDE). The process has an exponential covariance function and its discretized version is the famous AR(1) process. In the two dimensional spatial case, Whittle (1954) argues convincingly that the process with a Whittle correlation function is an “elementary” process (see Section 3.2 on a further discussion). If the time dimension is added, we think that the process defined below through the stochastic partial differential equation (SPDE) (1) has properties that make it a good candidate for an “elementary” spatio-temporal process. It is a linear equation that explicitly models phenomena such as transport and diffusion that occur in many natural processes ranging from environmental sciences to ecology. Furthermore, if no transport and diffusion occur, its covariance structure

reduces to a separable one with an AR(1) structure over time at each point in space and, depending on the specific choice, a certain covariance structure over space at each time point.

Consider the SPDE

$$\frac{\partial}{\partial t}\epsilon(t, \mathbf{s}) = -\boldsymbol{\mu} \cdot \nabla \epsilon(t, \mathbf{s}) + \nabla \cdot \boldsymbol{\Sigma} \nabla \epsilon(t, \mathbf{s}) - \zeta \epsilon(t, \mathbf{s}) + \xi(t, \mathbf{s}), \quad (1)$$

with $\mathbf{s} = (x, y)' \in \mathbb{R}^2$, where $\nabla = \left(\frac{\partial}{\partial x}, \frac{\partial}{\partial y}\right)'$ is the gradient operator, and $\nabla \cdot \mathbf{F} = \frac{\partial U}{\partial x} + \frac{\partial V}{\partial y}$ is the divergence operator, $\mathbf{F} = (U, V)'$ being a vector field. $\xi(t, \mathbf{s})$ is a Gaussian process that is temporally white and spatially colored. The concrete spatial structure of $\xi(t, \mathbf{s})$ is specified below in Section 3.2.

The SPDE has the following interpretation. Heuristically, an SPDE specifies what happens locally at each point in space during a very small time step. The first term $\boldsymbol{\mu} \cdot \nabla \epsilon(t, \mathbf{s})$ models transport effects (called advection in weather applications), $\boldsymbol{\mu}$ being a drift or velocity vector. The second term, $\nabla \cdot \boldsymbol{\Sigma} \nabla \epsilon(t, \mathbf{s})$, is a diffusion term that can incorporate anisotropy. When $\boldsymbol{\Sigma}$ is the identity matrix, this term reduces to the divergence ($\nabla \cdot$) of the gradient (∇) which is the ordinary Laplace operator $\nabla \cdot \nabla = \nabla^2 = \Delta = \frac{\partial^2}{\partial x^2} + \frac{\partial^2}{\partial y^2}$. Next, $-\zeta \epsilon(t, \mathbf{s})$ accounts for damping and regulates the amount of temporal correlation. Finally, $\xi(t, \mathbf{s})$ is a source-sink or stochastic forcing term that can be interpreted as describing convective phenomena in precipitation modeling applications.

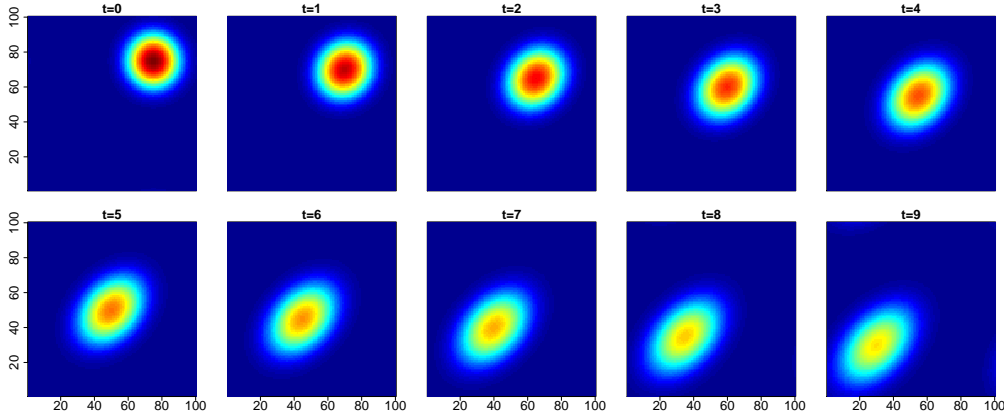


Figure 1. Illustration of deterministic part of the SPDE in (1) without stochastic term $\xi(t, \mathbf{s})$. The drift vector points from north-east to south-west and the diffusive part exhibits anisotropy in the same direction.

Figure 1 shows an illustration of the deterministic part of the SPDE in (1), i.e., the partial differential equation (PDE) that is obtained when there is no stochastic term $\xi(t, \mathbf{s})$. The figure shows how the initial state in the top-left plot gets propagated forward in time. The drift vector points from north-east to south-west and the diffusive part exhibits anisotropy in the same direction. A 100×100 grid is used and the PDE is solved in the spectral domain using the method described below in Section 3.

For illustrative purposes, Figure 2 shows one sample from the distribution specified by the SPDE in (1). As initial state distribution, we use a Dirac measure with point mass at the initial state of the deterministic example above, i.e., we use a fixed initial state. For the innovations $\xi(t, \mathbf{s})$, we use a Gaussian process that is temporally independent and spatially structured according to the Matérn covariance function with smoothness parameter 1. As in the previous example, the drift vector points from north-east to south-west and the diffusive part exhibits anisotropy in the same direction.

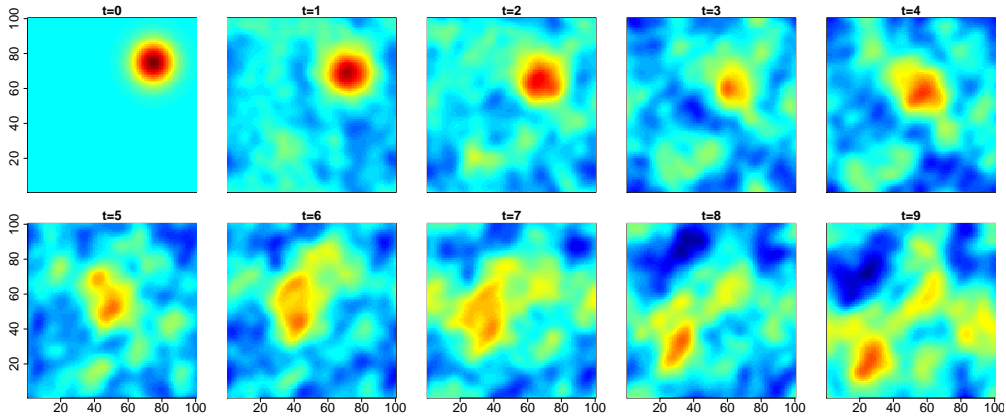


Figure 2. Illustration of the SPDE in (1). The figure shows one sample from the distribution specified by the SPDE. The drift vector points from north-east to south-west and the diffusive part exhibits anisotropy in the same direction.

As indicated in the introduction, there is a fundamental difference between the deterministic PDE and the probabilistic SPDE. In the first case, a deterministic process is modeled directly. In the second case, the SPDE defines a stochastic process. Since the operator is linear and the input Gaussian, this process is a Gaussian process. Therefore, it is completely specified by the mean and covariance function. The mean is zero and the covariance function is implicitly defined by the SPDE. In other words, the SPDE, or an approximate solution to the SPDE, can be seen as a tool to implicitly specify a reasonable parametrization for a covariance function of a Gaussian process in space and time.

Note that the use of this Gaussian process is not restricted to situations where it is a priori known that phenomena like transport and diffusion occur. In the one dimensional case, it is common to use the AR(1) process in situations where it is not a priori clear whether the modeled process follows the dynamic of the Ornstein-Uhlenbeck SDE. In two dimensions, the same holds true for the process with the Whittle covariance function, not to mention the process having an exponential covariance structure. Having this in mind, we think that even though the SPDE (1) is physically motivated, it can be used as a general spatio-temporal model. The interpretation of the parameters can then be less meaningful, though.

2.1 Relation to an Integro-Difference Equation

Assuming discrete time steps with lag distance Δ , Brown et al. (2000) consider the following integro-difference equation (IDE)

$$\epsilon(t, \mathbf{s}) = \exp(-\Delta\zeta) \int_{\mathbb{R}^2} h(\mathbf{s} - \mathbf{s}') \epsilon(t - \Delta, \mathbf{s}) d\mathbf{s}' + \xi(t, \mathbf{s}), \quad \mathbf{s} \in \mathbb{R}^2, \quad (2)$$

with a Gaussian redistribution kernel

$$h(\mathbf{s} - \mathbf{s}') = (2\pi)^{-1} |2\Delta\mathbf{\Sigma}|^{-1/2} \exp\left(-(\mathbf{s} - \mathbf{s}' - \Delta\boldsymbol{\mu})^T (2\Delta\mathbf{\Sigma})^{-1} (\mathbf{s} - \mathbf{s}' - \Delta\boldsymbol{\mu})/2\right), \quad (3)$$

$\xi(t, \mathbf{s})$ being temporally independent and spatially dependent. They show that in the limit $\Delta \rightarrow 0$, the solution of the IDE and the one of the SPDE in (1) coincide. Concerning interpretation of (2), the convolution kernel $h(\mathbf{s} - \mathbf{s}')$ determines the weight or the amount of influence that a location \mathbf{s}' at time $t - \Delta$ has on the point \mathbf{s} at time t . Having this in mind, the IDE representation can additionally help with the interpretation of the SPDE model and its parameters. Stordvik et al. (2002) show under which conditions a dynamic model determined by an IDE as in (2) can be represented using a parametric joint space-time covariance function, and vice versa. Based on the IDE in (2), Sigrist et al. (2012) construct a spatio-temporal model for irregularly spaced data and apply it to obtain short term predictions of precipitation.

2.2 Spectral Density and Covariance Function

As we show in Section 3, using the Fourier transform, the spectrum of a stationary solution $\epsilon(t, \mathbf{s})$ of the SPDE (1) is

$$f(\omega, \mathbf{k}) = \hat{f}(\mathbf{k}) \frac{1}{(2\pi)} \left((\mathbf{k}'\mathbf{\Sigma}\mathbf{k} + \zeta)^2 + (\omega + \boldsymbol{\mu}'\mathbf{k})^2 \right)^{-1}, \quad (4)$$

where $\hat{f}(\mathbf{k})$ is the spectral density of the innovation process, and where \mathbf{k} and ω are spatial wave numbers and temporal frequencies. Since, in general, this spectrum does not factorize into a temporal and a spatial component, we see that $\epsilon(t, \mathbf{s})$ has a non-separable covariance function (see Gneiting et al. (2007b) for a definition of separability). The model reduces to a separable one, though, when there is no advection and diffusion, i.e., when both $\boldsymbol{\mu}$ and $\mathbf{\Sigma}$ are zero.

The covariance function $C(t, \mathbf{s})$ of $\epsilon(t, \mathbf{s})$ is

$$C(t, \mathbf{s}) = \int f(\omega, \mathbf{k}) \exp(it\omega) \exp(i\mathbf{s}'\mathbf{k}) d\mathbf{k} d\omega. \quad (5)$$

This integral has in general no closed form solution but can be computed approximately by numerical integration.

3 Dimension Reduction in the Spectral Space

The solution $\epsilon(t, \mathbf{s})$ of the SPDE (1) is defined in continuous space and time. Even when the data are on a grid of N spatial locations combined with T discrete time points, the resulting vector is in general of large dimension. This

makes inference, be it frequentist or Bayesian, computationally difficult. One potential way to overcome these difficulties is using sparse matrix approximations resulting, for instance, from finite difference approximations. Unfortunately, in our case, this did not result to be satisfactory (see Section 3.5). The approach we propose here is to obtain dimension reduction by representing the process $\epsilon(t, \mathbf{s})$ as a linear combination of a small number of deterministic spatial basis functions $\phi_j(\mathbf{s})$ with random coefficients $\alpha_j(t)$ that evolve dynamically over time

$$\epsilon(t, \mathbf{s}) = \sum_{j=1}^K \alpha_j(t) \phi_j(\mathbf{s}) = \boldsymbol{\phi}(\mathbf{s})' \boldsymbol{\alpha}(t), \quad (6)$$

where $\boldsymbol{\phi}(\mathbf{s}) = (\phi_1(\mathbf{s}), \dots, \phi_K(\mathbf{s}))'$ and $\boldsymbol{\alpha}(t) = (\alpha_1(t), \dots, \alpha_K(t))'$.

It is advantageous to use Fourier functions

$$\phi_j(\mathbf{s}) = \exp(i\mathbf{k}_j' \mathbf{s}), \quad (7)$$

where i denotes the imaginary number $i^2 = -1$ and $\mathbf{k}_j = (k_j^x, k_j^y)'$ is a spatial wave number, since then differentiation in the physical space corresponds to multiplication in the spectral space. Because Fourier functions are eigenfunctions of the spatial differential operators, solutions to the SPDE in (1) stay in subspaces generated by a finite number of Fourier functions provided the forcing term $\xi(t, \cdot)$ belongs to the same subspace for all t . More precisely, we have the following result.

Proposition 1. *Assume that*

$$\epsilon(0, \mathbf{s}) = \boldsymbol{\phi}(\mathbf{s})' \boldsymbol{\alpha}(0), \quad \xi(t, \mathbf{s}) = \boldsymbol{\phi}(\mathbf{s})' \widehat{\boldsymbol{\xi}}(t) \quad (8)$$

where $\boldsymbol{\phi}(\mathbf{s}) = (\phi_1(\mathbf{s}), \dots, \phi_K(\mathbf{s}))'$ and $\widehat{\boldsymbol{\xi}}(t)$ is a K -dimensional complex-valued white noise independent of $\boldsymbol{\alpha}(0)$, that is

$$\text{Cov}(\widehat{\boldsymbol{\xi}}(t), \widehat{\boldsymbol{\xi}}(t')) = \delta_{t,t'} \mathbf{Q}.$$

Then the process $\epsilon(t, \mathbf{s}) = \boldsymbol{\phi}(\mathbf{s})' \boldsymbol{\alpha}(t)$ where the components $\alpha_j(t)$ are given by

$$\alpha_j(t) = \exp(h_j t) \alpha_j(0) + \int_0^t \exp(h_j(t-s)) \widehat{\xi}_j(s) ds \quad (9)$$

with $h_j = -i\boldsymbol{\mu}' \mathbf{k}_j - \mathbf{k}_j' \boldsymbol{\Sigma} \mathbf{k}_j - \zeta$ is a solution of the SPDE in (1). For $t \rightarrow \infty$, the influence of the initial condition $\exp(h_j t) \alpha_j(0)$ converges to zero and the process $\epsilon(t, \mathbf{s})$ converges to a stationary Gaussian process with mean zero and

$$\text{Cov}(\epsilon(t + \Delta t, \mathbf{s}), \epsilon(t, \mathbf{s}')) = \boldsymbol{\phi}(\mathbf{s})' \mathbf{Q}(\Delta t) \boldsymbol{\phi}(\mathbf{s}')^*$$

where * stands for complex conjugation and $\mathbf{Q}(\Delta t)$ is the matrix with elements $-\exp(h_j \Delta t) Q_{jl} / (h_j + h_l^*)$.

Proof of Proposition 1. By (9), we have

$$\sum_{j=1}^K \dot{\alpha}_j(t) \phi_j(\mathbf{s}) = \sum_{j=1}^K (h_j \alpha_j(t) + \widehat{\xi}_j(t)) \phi_j(\mathbf{s}). \quad (10)$$

On the other hand, since the functions $\phi_j(\mathbf{s}) = \exp(i\mathbf{k}'_j \mathbf{s})$ are Fourier terms, the differentiation in the physical space corresponds to multiplication in the spectral space:

$$\boldsymbol{\mu} \cdot \nabla \phi_j(\mathbf{s}) = i\boldsymbol{\mu}' \mathbf{k}_j \phi_j(\mathbf{s}) \quad (11)$$

and

$$\nabla \cdot \boldsymbol{\Sigma} \nabla \phi_j(\mathbf{s}) = -\mathbf{k}'_j \boldsymbol{\Sigma} \mathbf{k}_j \phi_j(\mathbf{s}). \quad (12)$$

Therefore by the definition of h_j

$$(-\boldsymbol{\mu} \cdot \nabla + \nabla \cdot \boldsymbol{\Sigma} \nabla - \zeta) \sum_{j=1}^K \alpha_j(t) \phi_j(\mathbf{s}) = \sum_{j=1}^K h_j \alpha_j(t) \phi_j(\mathbf{s}). \quad (13)$$

This proves the first part of the proposition. Since the real part of h_j is negative, $\exp(h_j t) \rightarrow 0$ for $t \rightarrow \infty$. Moreover,

$$\begin{aligned} \lim_{t \rightarrow \infty} \text{Cov}(\alpha_j(t + \Delta t), \alpha_l(t)) &= \lim_{t \rightarrow \infty} \exp(h_j \Delta t) Q_{jl} \int_0^t \exp(-(h_j + h_l^*)(t - s)) ds \\ &= -\frac{\exp(h_j \Delta t)}{h_j + h_l^*} Q_{jl}, \end{aligned} \quad (14)$$

and thus the last statement follows. \square

In order to obtain a real-valued solution $\epsilon(t, \mathbf{s})$, we require that together with any $\mathbf{k}_j \neq 0$ we also include $-\mathbf{k}_j$ and that $\widehat{\xi}_{j'} = \widehat{\xi}_j^*$ if $\mathbf{k}_{j'} = -\mathbf{k}_j$. Then we can work with sine and cosine instead of the complex exponential, see the discussion below in Section 3.3.

Proposition 1 can be used to construct a solution of the SPDE in (1) if the forcing term $\xi(t, \cdot)$ is stationary in space: By the Cramér representation

$$\xi(t, \mathbf{s}) = \int \exp(i\mathbf{k}' \mathbf{s}) d\Xi_t(\mathbf{k})$$

where Ξ_t has orthogonal increments $\text{Cov}(d\Xi_t(\mathbf{k}), d\Xi_{t'}(\mathbf{l})) = \delta_{t,t'} \delta_{\mathbf{k}, \mathbf{l}} \widehat{f}(\mathbf{k})$ and \widehat{f} is the spectral density of $\xi(t, \cdot)$. This implies that we can approximate such a ξ by a finite linear combination of complex exponentials as required in the proposition, and moreover the covariance Q of $\widehat{\xi}(t)$ can be chosen as a diagonal matrix. By passing to the limit, we then obtain the stationary (in space and time) solution with spectral density as in (4).

3.1 Discretization in Time and Space

In our application, we need the process $\epsilon(t, \mathbf{s})$ on a regular grid of $n \times n = N$ spatial locations $\mathbf{s}_1, \dots, \mathbf{s}_N$ and at equidistant time points t_1, \dots, t_T with $t_i - t_{i-1} = \Delta$. We therefore choose in the approximation frequencies of the form $\mathbf{k}_j = (k_j^x, k_j^y)'$, $k_j^x, k_j^y \in \{k \cdot 2\pi/n : k = -n/2 + 1, \dots, n/2\}$, $j = 0, \dots, K$.

In order to reduce the dimension, we consider values of K that are potentially a lot smaller than $N = n^2$, including only low frequencies. In a purely spatial setting, Paciorek (2007) states that “the most important basis functions for function estimation are the low-frequency basis functions”. We think that the same holds true in the spatio-temporal case. We thereby obtain an approximate model that is computationally tractable. The higher frequencies can be accounted for by an additional unstructured term which is usually called nugget effect in the geostatistical literature. This is done in our application in Section 4. Additionally, one can also add a term having spatial but no temporal correlation to account for small scale variation.

Since we would like our process $\epsilon(t, \mathbf{s})$ to be an approximation of the solution of the SPDE with a spatially stationary white noise with spectral density \hat{f} , we choose the covariance of the coefficients $\hat{\xi}$ as a diagonal matrix with elements $\hat{f}(\mathbf{k}_j)$. The choice of \hat{f} is discussed below in Section 3.2.

Proposition 1 then says that, under the assumptions in (8), the solution of the SPDE (1) is given by

$$\epsilon(t_{i+1}) = \Phi \alpha(t_{i+1}), \quad (15)$$

$$\alpha(t_{i+1}) = \mathbf{G} \alpha(t_i) + \tilde{\xi}(t_{i+1}), \quad \tilde{\xi}(t_{i+1}) \sim N(0, \tilde{\mathbf{Q}}), \quad (16)$$

where $\epsilon(t) = (\epsilon(t, \mathbf{s}_1), \dots, \epsilon(t, \mathbf{s}_N))'$, $\Phi = \{\phi(\mathbf{s}_1), \dots, \phi(\mathbf{s}_N)\}'$ applies the inverse discrete Fourier transformation,

$$\mathbf{G} = \exp(\Delta \cdot \mathbf{H}), \quad \mathbf{H} = \text{diag}(h_j), \quad (17)$$

and

$$\begin{aligned} \tilde{\mathbf{Q}} &= \int_t^{t+\Delta} \exp((t + \Delta - u) \cdot \mathbf{H}) \mathbf{Q} \exp((t + \Delta - u) \cdot \mathbf{H}') du \\ &= \text{diag} \left(\hat{f}(\mathbf{k}_j) \frac{\exp((h_j + h_j^*)\Delta) - 1}{h_j + h_j^*} \right). \end{aligned} \quad (18)$$

The above equations (15) and (16) form a linear Gaussian state space model with parametric propagator matrix \mathbf{G} and innovation covariance matrix $\tilde{\mathbf{Q}}$, the parametrization being determined by the corresponding SPDE. The dimensions of the latent state $\alpha(t)$, which determines computational cost, can be much lower than the dimension of $\epsilon(t)$. Furthermore, for calculating the inverse Fourier transform in (15), there is no need for matrix multiplication but one may use the fast Fourier transform (FFT) (Cooley and Tukey 1965) instead.

3.2 Specification of the Innovation Process

As mentioned before, it is assumed that the innovation process $\xi(t, \mathbf{s}) = \phi(\mathbf{s})' \hat{\xi}(t)$ is white in time and has a stationary covariance structure in space. We recall

that the function $\hat{f}(\cdot)$ specifies the variances of the different frequencies $\hat{\xi}_j(t)$, i.e., it determines the spatial spectrum of $\xi(t, \mathbf{s})$ and thus its covariance structure.

The spectrum $\hat{f}(\cdot)$ is chosen such that $\xi(t, \mathbf{s})$ approximates the process $\mathcal{Z}(t, \mathbf{s})$ which is white in time and has the Whittle covariance function in space. This covariance function is of the form $\sigma^2 \rho_0 d / 2K_1(d/\rho_0)$ with d being the Euclidean distance between two points and $K_1(d/\rho_0)$ being the modified Bessel function of order 1. It is called after Whittle (1954) who introduced it and argued convincingly that it “may be regarded as the ‘elementary’ correlation in two dimensions, similar to the exponential in one dimension.”. It has a long history in various fields (Guttorp and Gneiting 2006), and it is a special case of what Handcock and Stein (1993) termed the Matérn covariance function with smoothness parameter 1. It can be shown that the solution of the SPDE

$$\left(\nabla \cdot \nabla - \frac{1}{\rho_0^2} \right) \mathcal{Z}(t, \mathbf{s}) = \mathcal{W}(t, \mathbf{s}), \quad (19)$$

where $\mathcal{W}(t, \mathbf{s})$ is a zero mean Gaussian white noise field with variance σ^2 , has the Whittle covariance function in space. Based on this, it follows that the spectrum of the process $\mathcal{Z}(t, \mathbf{s})$ is given by

$$\hat{f}(\mathbf{k}) = \frac{\sigma^2}{(2\pi)^2} \left(\mathbf{k}'\mathbf{k} + \frac{1}{\rho_0^2} \right)^{-2}. \quad (20)$$

3.3 Real Fourier Functions

For the sake of simplicity, we have stated the above results using complex Fourier functions. The propagator matrix \mathbf{G} contains complex numbers, though. To avoid this, we replace the complex terms $\exp(i\mathbf{k}'_j \mathbf{s})$ with real $\cos(\mathbf{k}'_j \mathbf{s})$ and $\sin(\mathbf{k}'_j \mathbf{s})$ functions. All the results are then obtained in an analogous way, except that the matrix \mathbf{H} is no longer diagonal but block diagonal. The real basis functions share all the advantages that the complex ones have. In particular, they are eigen functions of the differential operator used in the SPDE, and the fast Fourier transform (FFT) can still be used for efficiently computing the transform from the spectral space to the physical space, and vice versa.

Since \mathbf{H} is neither diagonal nor symmetric, computation of the innovation covariance (18) is complicated, however. Hence, we approximate the stochastic innovation term using a first order approximation and replace (16) with

$$\boldsymbol{\alpha}(t + \Delta) = \mathbf{G}\boldsymbol{\alpha}(t) + \sqrt{\Delta} \cdot \hat{\boldsymbol{\xi}}(t + \Delta). \quad (21)$$

In the following, we briefly illustrate the use of real Fourier functions. For real valued data, the real Fourier transform is equivalent to the complex one. It uses the fact that certain coefficients of the complex transform are the complex transpose of other coefficients. This allows for expressing the complex coefficients in terms of their real and imaginary part, the real and imaginary parts of the complex amplitudes corresponding to the coefficients of the cosine and sine terms, respectively, in the real transform. For technical details, we refer to

Dudgeon and Mersereau (1984), Borgman et al. (1984), Royle and Wikle (2005), and Paciorek (2007). When using the real discrete Fourier transform, all of the above remains true, except that \mathbf{G} is block diagonal because the derivative of a cosine is a sine term and vice versa.

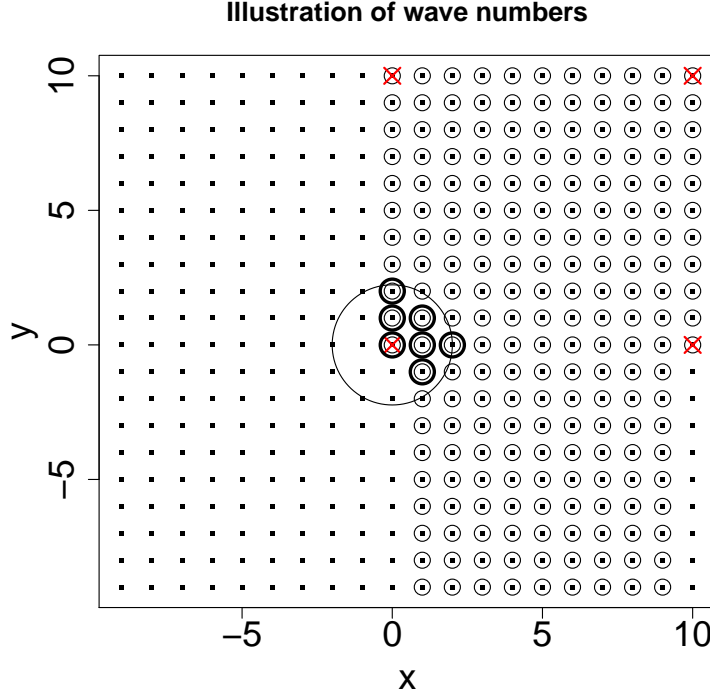


Figure 3. Illustration of wave numbers for the two-dimensional discrete real Fourier transform.

As an illustrative example, we consider a grid consisting of $n \times n$, $n = 20$, equidistant points. In Figure 3, each dot corresponds to a spatial frequency with associated wave number \mathbf{k}_j , and each wave number has a corresponding Fourier coefficient. Of all the $N = n^2$ complex coefficients, only those with a circle around them are unique due to the conjugate symmetry. In the real Fourier transform, each of these wave numbers \mathbf{k}_j with a circle has a corresponding cosine and sine coefficient, except for those four points with a red cross. Concerning these four wave numbers, the sine coefficients are zero and only the cosine coefficients are used.

In order to select the spatial frequencies in a dimension-reduced model, we chose a real number k and then use all \mathbf{k}_j for which

$$|\mathbf{k}_j| \leq k \frac{2\pi}{n}, \quad 0 < k \leq \frac{n}{\sqrt{2}}. \quad (22)$$

In Figure 3, $k = 2$ is shown. This is illustrated with the circle around $(0,0)'$ with radius 2. The spatial frequencies with a bold circle around them are the ones for which (22) holds true. These are the wave numbers that are included in the

spectral approximation. Notice that the spatial frequency at $(0, 0)'$ corresponds to a constant term.

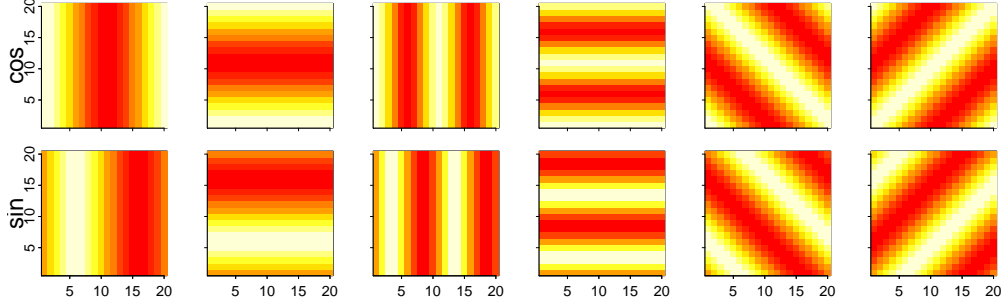


Figure 4. Illustration of two dimensional basis functions used in the discrete real Fourier transform. On the x- and y-axis are the coordinates of $\mathbf{s} = (s_x, s_y)'$.

To get an idea how the basis functions $\cos(\mathbf{k}'_j \mathbf{s})$ and $\sin(\mathbf{k}'_j \mathbf{s})$ look like, we plot in Figure 4 the 12 basis functions corresponding to the above spatial frequencies (excluding the constant term). On the x- and y-axis are the coordinates of $\mathbf{s} = (s_x, s_y)'$. The first six functions, from top left to bottom right, are cosine terms followed by sine terms.

In practice, in order to avoid spurious correlations resulting from periodicity when the correlation decay is slow relative to the size of the domain (see Paciorek (2007) for details), we apply what is called padding. This means that we embed the domain $n \times n$ in a larger domain of dimension $(2 \cdot n) \times (2 \cdot n)$, calculating but not using the values at the points that do not belong to the original domain $n \times n$.

3.4 Estimation

In practice, $\epsilon(t)$ is typically not observed without error, meaning that in the observation equation (15) Gaussian noise is added. Such a model can then be estimated using maximum likelihood estimation, or when following a Bayesian paradigm, posterior distributions can be calculated. Another possibility is to use this spatio-temporal model as a component in a larger Bayesian hierarchical model (BHM) (Wikle et al. 1998). Depending on the data model used in the BHM, a frequentist approach is no longer feasible since the marginal likelihood has no closed form expression and involves a high-dimensional integral. This is the case in our application. But approximate posterior probabilities can still be computed using simulation based methods such as Markov chain Monte Carlo (MCMC) (see, e.g., Gilks et al. (1996) or Robert and Casella (2004)) or deterministic ones such as the integrated nested Laplace approximation (INLA) (Rue et al. 2009). An additional advantage of BHMs is that these models can be easily extended, for instance, to account for temporal nonstationarity by letting one or several parameters vary over time. In our application, this is done by linking the drift term to an external wind vector (see Section 4.2).

3.5 Remarks on Finite Differences

Another approach to solve PDEs or SPDEs such as the one in (1) consists of using a discretization such as finite differences. Stroud et al. (2010) use finite differences to solve an advection-diffusion PDE. Other examples are Wikle (2003), Xu and Wikle (2007), Duan et al. (2009), Malmberg et al. (2008), and Zheng and Aukema (2010). The finite difference approximation, however, has several disadvantages. First, each spatial discretization effectively implies an interaction structure between temporal and spatial correlation. In other words, as Xu et al. (2005) state, the discretization effectively suggests a knowledge of the scale of interaction, lagged in time. Usually, this space-time interaction structure is not known, though. Furthermore, there are numerical stability conditions that need to be fulfilled in order that the approximate solution is meaningful. Since these conditions depend on the values of the unknown parameters, one can run into problems.

In addition, computational tractability is an issue. In fact, we have tried to solve the SPDE in (1) using finite differences as described in the following. Finite difference approximations in (1) leads to a vector autoregressive model with a sparse propagator matrix being determined by the discretization. The innovation term ξ , for instance defined through the SPDE (19), can be approximated using a Gaussian Markov random field with sparse precision matrix (see Lindgren et al. (2011)). Even though the propagator and the precision matrix of the innovations are sparse, we have run into a computational bottleneck when using the Forward Filtering Backward Sampling (FFBS) algorithm (Carter and Kohn 1994; Frühwirth-Schnatter 1994) which is used when fitting the model. The basic problem is that the Kalman gain is eventually a dense matrix. Alternative sampling schemes like the information filter (see, e.g., Anderson and Moore (1979) and Vivar and Ferreira (2009)) did not solve the problem either. However, future research on this topic might come up with solutions.

4 Modeling Precipitation

The model presented in the following is a Bayesian hierarchical model (BHM). It uses the spatio-temporal process presented above at the process level. At the data stage, a model adapted to the nature of precipitation is used. This data model is presented in the following.

4.1 Data Model

A characteristic feature of precipitation is that its distribution consists of a discrete component, indicating occurrence of precipitation, and a continuous one, determining the amount. As a consequence, there are two basic statistical modeling approaches. The continuous and the discrete part are either modelled separately (Coe and Stern 1982; Wilks 1999) or together (Bell 1987; Wilks 1990; Bardossy and Plate 1992; Hutchinson 1995; Sanso and Guenni 2004). See Sigrist et al. (2012) for a more extensive overview of precipitation models and for further details on the data model used below. Originally, the approach

presented in the following goes back to Tobin (1958) who analyzed household expenditure on durable goods. For modeling precipitation, Stidd (1973) took up this idea and modified it by including a power-transformation for the non-zero part so that the model can account for skewness.

It is assumed that the rainfall $Y(t, \mathbf{s})$ at time t on site $\mathbf{s} = (x, y)' \in \mathbb{R}^2$ depends on a latent normal variable $W(t, \mathbf{s})$ through

$$\begin{aligned} Y(t, \mathbf{s}) &= 0, & \text{if } W(t, \mathbf{s}) \leq 0, \\ &= W(t, \mathbf{s})^\lambda, & \text{if } W(t, \mathbf{s}) > 0, \end{aligned} \quad (23)$$

where $\lambda > 0$. A power transformation is needed since precipitation amounts are skewed and do not follow a truncated normal distribution. The latent variable $W(t, \mathbf{s})$ can be interpreted as a precipitation potential.

The mean of $W(t, \mathbf{s})$ is assumed to depend linearly on covariates $\mathbf{x}(t, \mathbf{s}) \in \mathbb{R}^k$. Variation that is not explained by the linear term is modeled using the Gaussian process defined in the previous section and an additional term $\nu(t, \mathbf{s})$ that represents microscale variability and measurement errors. The model is then

$$W(t, \mathbf{s}) = \mathbf{x}(t, \mathbf{s})^T \mathbf{b} + \epsilon(t, \mathbf{s}) + \nu(t, \mathbf{s}), \quad (24)$$

where $\mathbf{b} \in \mathbb{R}^k$ and $\nu(t, \mathbf{s}) \sim N(0, \tau^2)$, $\tau^2 > 0$, are independent and identically distributed normal random variables. Since, in our application, we think that the resolution of the data does not allow for distinguishing between microscale variability and measurement errors, we model these two sources of variation together. Note that the covariates $\mathbf{x}(t, \mathbf{s})$ will usually be time and location dependent.

4.2 Specific Parametrization for the Latent Process

As mentioned above, we assume that the latent process $\epsilon(t, \mathbf{s})$ is specified by the SPDE in (1), or more specifically, the approximation in (15) and (21). Since we have information on wind, we relate the drift parameter $\boldsymbol{\mu}$ to the wind. This means that, for each t , we calculate an average wind vector $\mathbf{w}(t)$. Then we assume that

$$\boldsymbol{\mu}(t) = \omega \cdot \mathbf{w}(t) + (\mu_x, \mu_y)'. \quad (25)$$

Concerning the diffusion matrix $\boldsymbol{\Sigma}$, we use the following parametrization

$$\boldsymbol{\Sigma}^{-1} = \frac{1}{\rho_1^2} \begin{pmatrix} \cos \alpha & \sin \alpha \\ -\gamma \cdot \sin \alpha & \gamma \cdot \cos \alpha \end{pmatrix}^T \begin{pmatrix} \cos \alpha & \sin \alpha \\ -\gamma \cdot \sin \alpha & \gamma \cdot \cos \alpha \end{pmatrix} \quad (26)$$

The parameters are interpreted as follows. ρ_1 acts as a range parameter and controls the amount of diffusion. The parameters γ and α control the amount and the direction of anisotropy. With $\gamma = 1$, isotropic diffusion is obtained.

We thus obtain a temporally nonstationary model having a nonseparable covariance structure. The model reduces to one with a separable covariance function if both the drift term and the diffusion term equal zero, i.e., if

$$\boldsymbol{\Sigma} = \mathbf{0} \quad \text{and} \quad \boldsymbol{\mu}(t) = \mathbf{0}. \quad (27)$$

As mentioned, the covariance matrix $\Delta\widehat{\mathbf{Q}}$ of the spectral innovations is a diagonal matrix with entries

$$\widehat{Q}_{ii} = \frac{\sigma^2}{(2\pi)^2} \left(\mathbf{k}'_{j(i)} \mathbf{k}_{j(i)} + \frac{1}{\rho_0^2} \right)^{-2}, \quad (28)$$

where $\mathbf{k}_{j(i)}$ denotes the wavenumber of the corresponding cosine or sine term. The marginal variance of the innovations $\boldsymbol{\xi}(t)$ equals the sum over the power spectrum $\sum_i \widehat{Q}_{ii}$. For the sake of interpretability, we reparametrize σ^2 by dividing it by $\sum_i \widehat{Q}_{ii}$, so that the reparametrized variance parameter σ'^2 equals the marginal variance of the innovations $\boldsymbol{\xi}(t)$. For notational convenience, we will denote this reparametrized parameter by σ^2 henceforth.

5 Fitting

Monte Carlo Markov Chain (MCMC) is used to sample from the posterior distribution. To be more specific, we apply what Neal and Roberts (2006) call a Metropolis within-Gibbs algorithm which alternates between blocked Gibbs (Gelfand and Smith 1990) and Metropolis (Metropolis et al. 1953; Hastings 1970) sampling steps. For the random walk Metropolis steps, we use an adaptive algorithm (Roberts and Rosenthal 2009) meaning that the proposal covariances are successively estimated such that an optimal scaling is obtained with an acceptance rate between 0.2 and 0.3. See Roberts and Rosenthal (2001) for more information on optimal scaling for Metropolis-Hastings algorithms.

We assume that we have $T \times M$ observations $Y(t_j, \mathbf{s}'_i)$ at times t_1, \dots, t_T and locations $\mathbf{s}'_1, \dots, \mathbf{s}'_M$. We introduce an incidence matrix \mathbf{I} to select the latent grid process $\boldsymbol{\epsilon}_t$ at these stations. Missing values can either be dealt with by making \mathbf{I} time varying or by using a data augmentation approach. We adopt the latter (see Sigrist et al. (2012) for more details). In vector notation, the full model is then

$$\begin{aligned} \mathbf{Y}(t_j) &= \max(\mathbf{0}, \mathbf{W}(t_j))^\lambda, \\ \mathbf{W}(t_j) &= \mathbf{X}(t_j)\mathbf{b} + \mathbf{I}\boldsymbol{\Phi}\boldsymbol{\alpha}(t_j) + \boldsymbol{\nu}(t_j), \quad \boldsymbol{\nu}(t_j) \sim N(\mathbf{0}, \tau^2 \cdot \mathbb{I}), \\ \boldsymbol{\alpha}(t_j) &= \mathbf{G}(t)\boldsymbol{\alpha}(t_{j-1}) + \sqrt{\Delta} \cdot \widehat{\boldsymbol{\xi}}(t_j), \quad \widehat{\boldsymbol{\xi}}(t_j) \sim N(\mathbf{0}, \widehat{\mathbf{Q}}), \end{aligned} \quad (29)$$

where, e.g., $\mathbf{W}(t_j) = (W(t_j, \mathbf{s}'_1), \dots, W(t_j, \mathbf{s}'_M))'$ and the other vectors are defined analogously, and where $\mathbf{0}$ is a vector of zeros. $\mathbf{X}(t_j)$ is the matrix of covariates with rows corresponding to the different locations. The propagator matrix $\mathbf{G}(t)$ is now time dependent because the external wind drift vector varies over time. As mentioned above, $\boldsymbol{\Phi}$ applies the inverse Fourier transform that maps the process from the frequency domain to the original domain, and \mathbf{I} is an incidence matrix that relates the process on the grid to the observation locations. We assign non-informative improper priors to \mathbf{b} and λ by taking the Lebesgue measure on \mathbb{R} and \mathbb{R}_+ , respectively. The choice of priors for the other parameters $\sigma^2, \rho_0, \omega, \mu_x, \mu_y, \rho_1, \gamma, \alpha, \zeta$, and τ^2 is application dependent. It is discussed in Section 6.2.

We denote by α the set of all random coefficients $\alpha_i(t_j)$, and ϵ and \mathbf{W} are defined in an analogous way. Further, θ denotes the vector of hyperparameters that parametrize the α process plus τ^2 , i.e., $\theta = (\sigma^2, \rho_0, \omega, \mu_x, \mu_y, \rho_1, \gamma, \alpha, \zeta, \tau^2)$. Our goal is to simulate from the posterior distribution $[\mathbf{b}, \lambda, \theta, \alpha, \mathbf{W} | \mathbf{Y}]$, where \mathbf{Y} denotes the set of all observations. Note that for those observations with $Y(t_j, \mathbf{s}_i) > 0$, $W(t_j, \mathbf{s}_i)$ is completely determined when λ is known. For all other time and space points, with observations censored at zero or missing, we use a data augmentation approach (see Sigrist et al. (2012) for more details).

In the following, we use the notation " $y|\cdot$ " and " $P[y|\cdot]$ " to denote conditional distributions and densities, respectively. Sampling from the full conditional $[\mathbf{b}|\cdot]$ is done using a Gibbs step, the full conditional being a Gaussian distribution. For sampling from $[\lambda|\cdot]$, a random walk Metropolis step is used. Further, for sampling those values of \mathbf{W} corresponding to zero observations and missing values, a Gibbs step is applied, the full conditionals being truncated and regular Gaussian distributions, respectively.

Concerning θ and α , one can sample from $[\theta|\cdot]$ using a Metropolis step and from $[\alpha|\cdot]$ using the forward filtering backward sampling (FFBS) (Carter and Kohn 1994; Frühwirth-Schnatter 1994). It turns out that α and θ can be strongly dependent. Consequently, if one samples successively from $[\theta|\cdot]$ and $[\alpha|\cdot]$, one can run into slow mixing properties because, in each step, $[\theta|\cdot]$ is constrained by the latent process, and vice versa. This problem is analogous to the one observed when doing inference for diffusion models by introducing latent points (see, e.g., Roberts and Stramer (2001) and Golightly and Wilkinson (2008)). To circumvent this problem, we sample jointly from $[\theta, \alpha|\cdot]$. A proposal (θ^*, α^*) is obtained by sampling θ^* from a Gaussian distribution with the mean equaling the last value and an appropriately chosen covariance matrix and then sampling α^* from $[\alpha|\theta^*, \cdot]$. The second step can be done using the FFBS. The acceptance probability then equals

$$\min \left(1, \frac{P[\theta^*, \alpha^* | \mathbf{W}^{(i)}, \cdot] \cdot Q[\theta^{(i)}, \alpha^{(i)} | \theta^*, \alpha^*]}{P[\theta^{(i)}, \alpha^{(i)} | \mathbf{W}^{(i)}, \cdot] \cdot Q[\theta^*, \alpha^* | \theta^{(i)}, \alpha^{(i)}]} \right), \quad (30)$$

where $P[\cdot|\cdot]$ and $Q[\cdot|\cdot]$ denote full conditional and proposal densities, respectively. Fortunately, this ratio simplifies as described in the following. The full conditional factorizes as

$$P[\theta^*, \alpha^* | \mathbf{W}^{(i)}, \cdot] = P[\alpha^* | \theta^*, \mathbf{W}^{(i)}, \cdot] \cdot P[\theta^* | \mathbf{W}^{(i)}, \cdot], \quad (31)$$

and the proposal density is, as explained above,

$$Q[\theta^*, \alpha^* | \theta^{(i)}, \alpha^{(i)}] = P[\alpha^* | \theta^{(i)}, \alpha^{(i)}, \mathbf{W}^{(i)}] \cdot Q[\theta^* | \theta^{(i)}]. \quad (32)$$

Consequently, since the full conditional of α^* equals its proposal density, these two terms cancel in the fraction (30). Further, the term $Q[\theta^* | \theta^{(i)}]$ is a symmetric Gaussian density which then also cancels in (30). In the end, the ratio simplifies to

$$\min \left(1, \frac{P[\theta^* | \mathbf{W}^{(i)}]}{P[\theta^{(i)} | \mathbf{W}^{(i)}]} \right), \quad (33)$$

where $P[\boldsymbol{\theta}|\mathbf{W}^{(i)}]$ denotes the value of the density of $\boldsymbol{\theta}$ given the current $\mathbf{W}^{(i)}$ evaluated at $\boldsymbol{\theta}$, and where $\boldsymbol{\theta}^*$ and $\boldsymbol{\theta}^{(i)}$ denote the proposal and the last value of $\boldsymbol{\theta}$, respectively. We see that the acceptance ratio (30) does not depend on $\boldsymbol{\alpha}$. Thus, the parameters $\boldsymbol{\theta}$ are allowed to move faster in the parameter space. Note that the value of $P[\boldsymbol{\theta}^*|\mathbf{W}^{(i)}]$ is obtained as a side product of the Kalman filter in the FFBS.

When the dimension of the observed process is high, it is preferable not to use an incidence matrix \mathbf{H} and treat locations where no observations are made as missing values. To obtain a computationally fast FFBS algorithm, one can then use the orthonormality of the Fourier basis functions, i.e., $\boldsymbol{\Phi}'\boldsymbol{\Phi} = \mathbb{I}$, and the Woodbury matrix identity (Woodbury 1950) in the calculation of the Kalman gain. Further, multiplications with $\boldsymbol{\Phi}$ need not be done explicitly but one can use the FFT instead.

6 Postprocessing Precipitation Forecasts

Nowadays, numerical weather prediction (NWP) models are capable of producing predictive fields at spatially and temporally high frequencies. Statistical postprocessing serves two purposes. First, probabilistic predictions are obtained in cases where only deterministic ones are available. Further, even if “probabilistic” forecasts in form of ensembles (Palmer 2002; Gneiting and Raftery 2005) are available, they are typically not calibrated, i.e., they are often underdispersed (Hamill and Colucci 1997). The goal of postprocessing is then to obtain calibrated and sharp predictive distributions (see Gneiting et al. (2007a) for a definition of calibration and sharpness). In the case of precipitation, the need for postprocessing is particularly strong, since, despite their importance, precipitation forecasts are still not as accurate as forecasts for other meteorological quantities (Applequist et al. 2002; Stensrud and Yussouf 2007).

Several approaches for postprocessing precipitation forecasts have been proposed, including linear regression (Antolik 2000), logistic regression (Hamill et al. 2004), quantile regression (Bjørnar Bremnes 2004; Friederichs and Hense 2007), hierarchical models based on prior climatic distribution (Krzysztofowicz and Maranzano 2006), neural networks (Ramrez et al. 2005), and binning techniques (Yussouf and Stensrud 2006). Sloughter et al. (2007) propose a two-stage model to postprocess precipitation forecasts. Berrocal et al. (2008) extended the model of Sloughter et al. (2007) by accounting for spatial correlation. Kleiber et al. (2011) present a similar model that includes ensemble predictions and accounts for spatial correlation.

Except for the last two references, spatial correlation is typically not modeled in postprocessing precipitation forecasts, and none of the aforementioned models explicitly accounts for spatio-temporal dependencies. However, for temporally and spatially highly resolved data, it is necessary to account for correlation in space and time. First, spatio-temporal correlation is important, for instance, for predicting precipitation accumulation over space and time with accurate estimates of precision. Further, it is likely that errors of NWP models exhibit structured behaviour over space and time. A spatio-temporal model

can capture structured dynamics of this error term and extrapolate a spatial error over time.

In the following, we apply the model presented above to postprocess spatially and temporally highly resolved precipitation forecasts. The NWP model forecasts are deterministic and ensembles are not available in our case. The extension to use an ensemble instead of just one member can be easily done. One can include all the ensemble members in the regression part of the model. Or, in the case of unidentifiable members, one can use the location and the spread of the ensemble.

6.1 Data

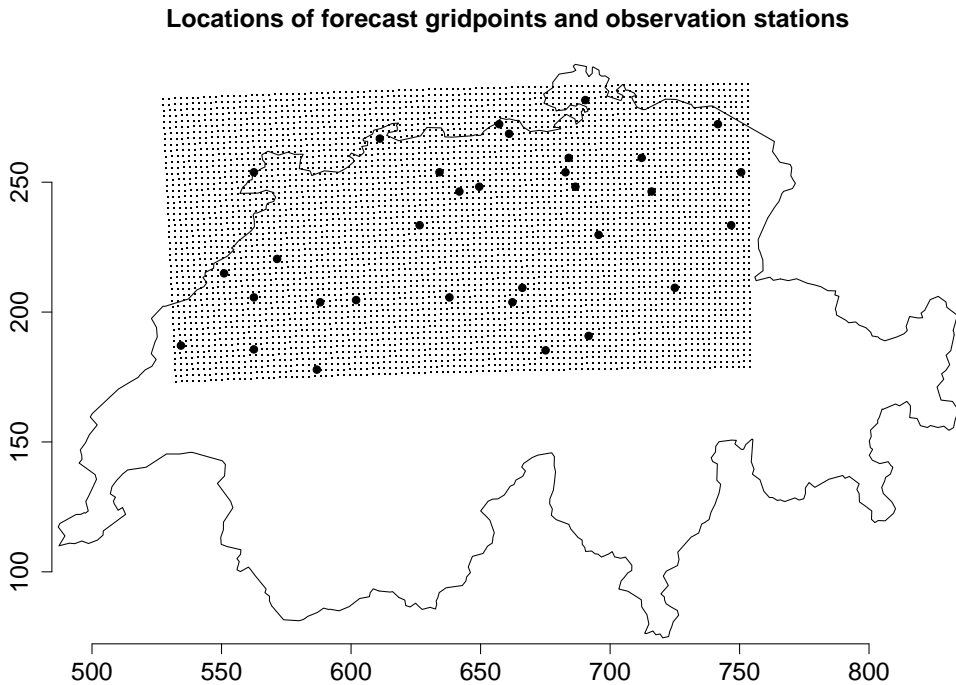


Figure 5. Locations of grid points at which predictions are obtained (50×100 grid of small dots) and observations stations (bold dots). Both axis are in km using the Swiss coordinate system (CH1903).

We have precipitation predictions from an NWP model called COSMO-2, a high-resolution model with a grid spacing of 2.2 km that is run by MeteoSwiss as part of COnsortium for Small-scale MOdelling (COSMO) (see, e.g., Steppeler et al. 2003). The NWP model produces predictions once a day starting at 0:00UTC. Predictions are made for eight consecutive time periods corresponding to 24 h ahead. $y_F(t, \mathbf{s})$ denotes the forecast for time t and site \mathbf{s} made at 0:00UTC of the same day. We consider a rectangular region in northern Switzerland shown in Figure 5. The grid at which predictions are made is of

size 50×100 . The figure also shows the locations of stations where precipitation is observed. We use three hourly data from the beginning of December 2008 till the end of March 2009. The first three months containing 720 time points are used for fitting and the last month is left aside for evaluation. In Figure 6, observed precipitation at one station and the (unweighted) areal average precipitation are plotted versus time.

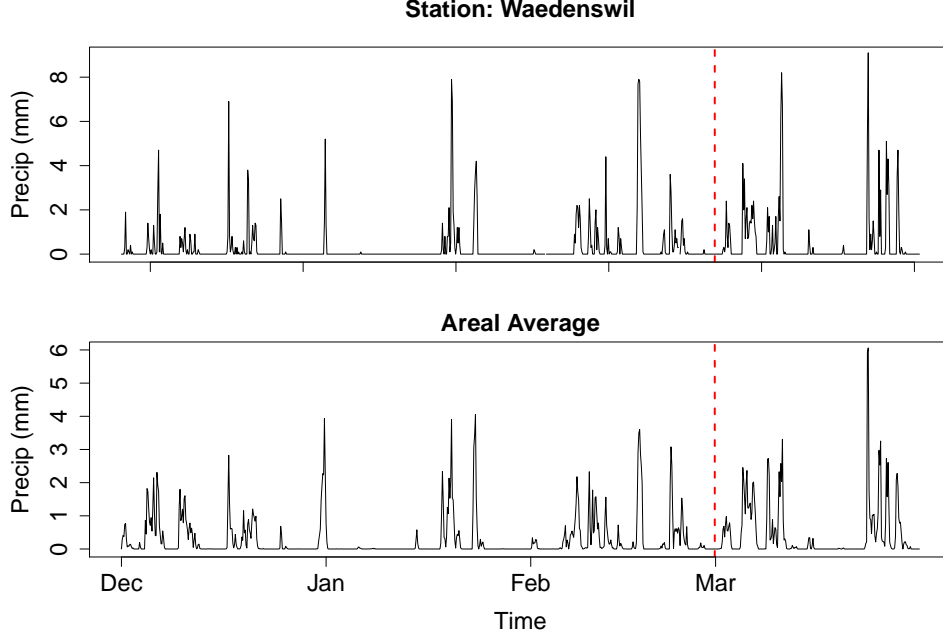


Figure 6. Precipitation versus time, for a specific station and averaged over all stations.

For modeling the mean in the latent model, we use two spatio-temporal covariates based on the NWP model predictions. Similarly as in Berrocal et al. (2008), we include a transformed variable $y_F(t, \mathbf{s})^{1/\tilde{\lambda}}$ and an indicator variable $\mathbf{1}_{\{y_F(t, \mathbf{s})=0\}}$ which equals 1 if $y_F(t, \mathbf{s}) = 0$ and 0 otherwise. $\tilde{\lambda}$ is determined by fitting the transformed Tobit model as in (23) to the marginal distribution of the rain data ignoring any spatio-temporal correlation. In doing so, we obtain $\tilde{\lambda} \approx 1.4$. Alternatively, $\tilde{\lambda}$ can also just assumed to be fix. For instance, Berrocal et al. (2008), use $\tilde{\lambda} = 3$. $y_F(t, \mathbf{s})^{1/\tilde{\lambda}}$ is centered around zero by subtracting its overall mean $\bar{y}_F^{1/\tilde{\lambda}}$ in order to reduce posterior correlations. Thus, $W(t, \mathbf{s})$ equals

$$W(t, \mathbf{s}) = b_1 \left(y_F(t, \mathbf{s})^{1/\tilde{\lambda}} - \bar{y}_F^{1/\tilde{\lambda}} \right) + b_2 \mathbf{1}_{\{y_F(t, \mathbf{s})=0\}} + \epsilon(t, \mathbf{s}) + \nu(t, \mathbf{s}). \quad (34)$$

An intercept is not included since the first Fourier term is constant in space. In our case, including an intercept term results in weak identifiability which slows down the convergence of the MCMC algorithm. Note that in situations where the mean is large it is advisable to include an intercept, since the coefficient of the first Fourier term is constrained by the joint prior on $\boldsymbol{\alpha}$. Further, unidentifiability is unlikely to be a problem in these cases.

6.2 Fitting

In the following, we use the width of a grid box as spatial unit, meaning that all the spatial quantities need to be multiplied by 2.2 to convert them to a km scale. Concerning padding, we embed the 50×100 grid in a rectangular 200×200 grid.

We assign the following almost non-informative priors to the parameters θ . For σ^2 and τ^2 we assume Gamma priors with mean 1 and variance 100. ω , μ_x , and μ_y have normal priors with mean 0 and variance 10^5 . α has a uniform prior on $[0, \pi/2]$ and γ has a uniform prior on $[0.1, 10]$. Furthermore, ρ_0 and ρ_1 have Gamma priors with mean 30 and variance 10^4 . Finally, ζ has a Gamma prior with mean 0.1 and variance 10^2 . γ is restricted to $[0.1, 10]$ since stronger anisotropy does not seem reasonable. The other priors were assigned prior means that seemed physically reasonable and relatively high variances so that they are little informative.

We then sample from the posterior distribution using the MCMC algorithm described in Section 5. After a burn-in of 5,000 iterations, we use 100,000 samples from the Markov chain to characterize the posterior distribution. Convergence is monitored by inspecting trace plots. We fit models with increasing numbers of basis functions choosing $k = 1, 1.5, 2, 2.5, 3, 3.5$, and 4 (see equation (22)).

6.3 Model Selection and Results

Having samples from the posterior distribution, we can generate samples from the predictive distribution. First, this is done in order to determine which model is the most appropriate, i.e., how many basis functions should be included. We then illustrate the application of the model to generate predictive forecasts.

Samples from the predictive distribution for the 240 time points that were set aside are obtained as follows. Ideally, one would run the full MCMC algorithm at each time point, including all data up to the point, and obtain predictive distributions from this. Since this is rather time consuming, we make the following approximation. We assume that the posterior distribution of the “primary” parameters θ , \mathbf{b} , and λ given $\mathbf{Y}_{1:t} = \{\mathbf{Y}_1, \dots, \mathbf{Y}_t\}$ is the same for all $t \geq 720$. That is, we neglect the additional information that the observations in March give about the primary parameters. In practice, this means that posterior distributions of the primary parameters are calculated only once, namely on the dataset from December 2008 to February 2009.

For each time point $t \geq 720$, we make up to 8 steps ahead forecasts corresponding to 24 hours. I.e., we sample from the predictive distribution of \mathbf{Y}_{t+k}^* , $k = 1, \dots, 8$, given $\mathbf{Y}_{1:t} = \{\mathbf{Y}_1, \dots, \mathbf{Y}_t\}$ and given the posterior of the primary parameters based on the data from December 2008 to February 2009.

The assumption that the posterior of the primary parameters does not change with additional data may be questionable over longer time periods and when one moves away from the time period from which data is used to obtain the posterior distribution. But since all our data lies in the winter season, we think that this assumption is reasonable. If longer time periods are considered,

one could use sliding training windows or model the primary parameters as non-stationary using a temporal evolution.

In order to assess the performance of the predictions and to choose the number of basis functions to include, we use the continuous ranked probability score (CRPS) (Matheson and Winkler 1976). The CRPS is a strictly proper scoring rule (Gneiting and Raftery 2007) that assigns a numerical value to probabilistic forecasts and assesses calibration and sharpness simultaneously (Gneiting et al. 2007a). It is defined as

$$CRPS(F, y) = \int_{-\infty}^{\infty} (F(x) - \mathbf{1}_{\{y \leq x\}})^2 dx, \quad (35)$$

where F is the predictive cumulative distribution, y is the observed realization, and $\mathbf{1}$ denotes an indicator function. It can be equivalently calculated as

$$CRPS(F, y) = E_F|Y - y| - \frac{1}{2}E_F|Y - Y'|, \quad (36)$$

where Y and Y' are independent random variables with distribution F . If a sample $Y^{(1)}, \dots, Y^{(m)}$ from F is available, it can be approximated by

$$\frac{1}{m} \sum_{i=1}^m |Y^{(i)} - y| - \frac{1}{2m^2} \sum_{i,j=1}^m |Y^{(i)} - Y^{(j)}|. \quad (37)$$

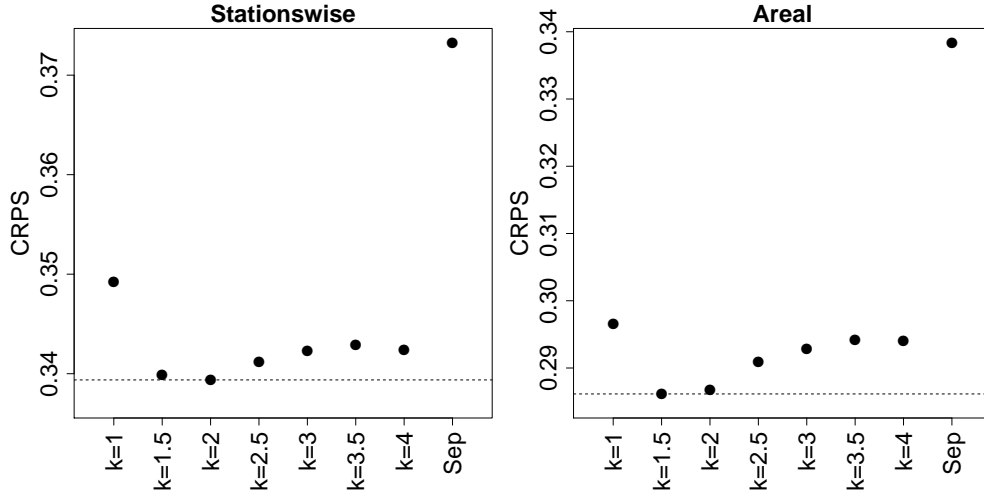


Figure 7. Comparison of different statistical models using the continuous ranked probability score (CRPS). On the left are CRPSs of station specific forecasts and on the right are CRPSs of areal forecasts. k determines the number of basis functions used in the model (see equation 22). “Sep” denotes the separable model with $k = 2$. The unit of the CRPS is mm.

In Figure 7, the average CRPS of the pointwise predictions and the areal predictions are shown for the different statistical models. In the left plot, the mean is taken over all stations and lead times, whereas the areal version is an

average over all lead times. This is done for the models with different numbers of basis functions used as well as for a separable model which is obtained by setting $\boldsymbol{\mu}(t) = \mathbf{0}$ and $\boldsymbol{\Sigma}^{-1} = \mathbf{0}$. The model with $k = 1$, corresponding to only 5 basis function, performs worse than the others. The models with $k = 1.5$ and $k = 2$ perform best. Subsequently adding more basis functions does not improve predictive performance. However, except for $k = 1$, the performance of the different models is not all too much different. In particular, there is not one single model that performs consistently better for all lead times (results not shown). The separable model with $k = 2$, on the other hand, clearly performs worse than the models with non-separable covariance structures. Based on these findings, we decide to use the model with $k = 2$ in the following. This corresponds to a model with 13 cosine and sine basis functions.

Table 1. Posterior means and 95 % credible intervals.

| | Mean | 2.5 % | 97.5 % |
|--|---------|----------|--------|
| $\mathbf{1}_{\{y_F(t,\mathbf{s})=0\}}$ | -0.42 | -0.497 | -0.347 |
| $y_F(t, \mathbf{s})$ | 0.442 | 0.41 | 0.474 |
| λ | 1.66 | 1.63 | 1.7 |
| τ^2 | 0.338 | 0.32 | 0.36 |
| σ^2 | 0.523 | 0.444 | 0.594 |
| ρ_0 | 8.8 | 0.201 | 12.9 |
| ζ | 0.00911 | 3.91e-07 | 0.0255 |
| ρ_1 | 17.8 | 14.7 | 20.6 |
| γ | 4.87 | 2.29 | 9.46 |
| α | 0.495 | 0.402 | 0.617 |
| ω | 0.0435 | -0.19 | 0.309 |
| μ_x | 3.38 | 1.22 | 5.58 |
| μ_y | -2.01 | -3.82 | -0.132 |

Table 1 shows posterior means as well as 95% credible intervals for the different parameters. The posterior mean of the nugget variance τ^2 is about 0.3 and the variance σ^2 of the innovations of the spatio-temporal process is around 0.5. For the innovation range parameter ρ_0 , we obtain about 9 grid spacings or $2.2 \times 9 = 20$ km. The effective range is therefore roughly $3 \times 20 = 60$ km. Having in mind the IDE representation (2), the range parameter ρ_1 that controls the amount of diffusion or, in other words, the amount of spatio-temporal interaction, has an effective range of about $\sqrt{3} \times 2 \times 2.2 \times 17.8 = 136$ km. Furthermore, the damping parameter ζ has a posterior mean of about 0.01. With γ and α being approximately 5 and 0.5, respectively, we observe strong anisotropy in the south-west to north-east direction. This is in line with the orography of the region, as the majority of the grid points lies between two mountain ranges: the Jura to the north-west and the Alps to the south-east. Concerning the drift, the wind regression parameter ω is close to zero. The rest of the drift, i.e., the constant part, points to the south-east.

Next, we compare the performance of the postprocessed forecasts with the

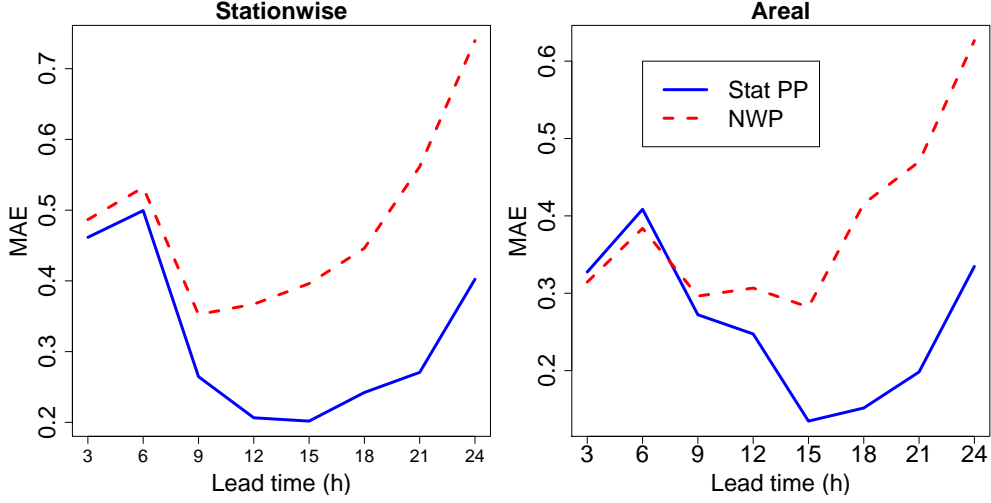


Figure 8. Comparison of NWP model and statistically postprocessed forecasts using the mean absolute error (MAE). Evaluation is done at 6 randomly selected stations which were removed from the data to fit the model. The unit of the MAE is mm.

ones from the NWP model. In addition to the temporal cross-validation where evaluation is done at the locations that were used to fit the model, we do the following cross-validation. We first remove 6 randomly selected stations from the data and fit the latent process to the remaining 26 stations. Evaluation of the forecasts is then done only at the selected 6 stations. Concerning the primary parameters, i.e., all parameters except the latent process, we still use the posterior obtained from the full data. This is done for computational simplicity and since this posterior is not very sensitive when excluding 6 stations. Thus, cross validation is not just done in time but also in space.

Since the NWP produces 8 step ahead predictions once a day, we only consider statistical forecasts starting at 0:00UTC. This is in contrast to the above comparison of the different statistical models for which 8 step ahead predictions were made at all time points. Furthermore, we use the mean absolute error (MAE) for evaluating the NWP forecasts. In order to be consistent, we also generate point forecasts from the statistical predictive distributions by using medians, and then calculate the MAE for these point forecasts. Figure 8 illustrates the results. The postprocessed forecasts clearly perform better than the raw NWP forecasts. In addition, the postprocessed forecasts have the advantage that they provide probabilistic forecasts quantifying prediction uncertainty. Note that there is one particular day (March 24) when heavy rainfall occurred shortly after 0:00UTC. The relatively high MAEs of the NWP, and also the postprocessed forecasts, for short lead times is due to this event. Excluding March 24, we obtain considerably lower MAE values for lead times 3h and 6h (results not shown).

Having selected a model, we can generate various predictive quantities. As an example, we consider the time point $t = 760$ and calculate predictive distri-

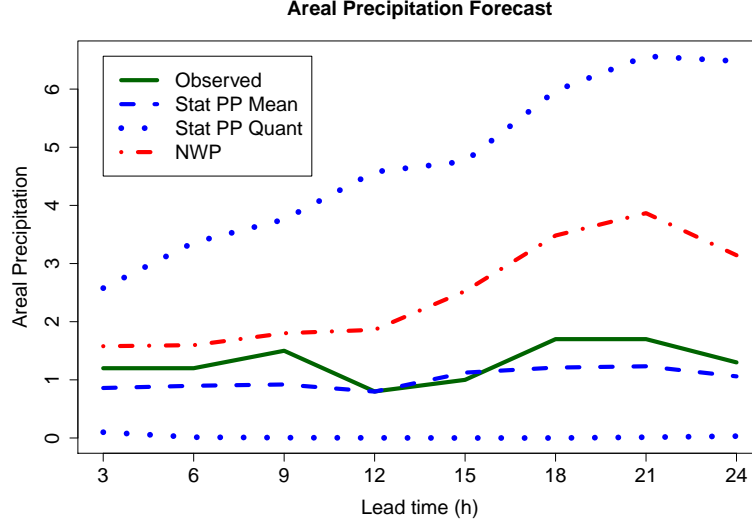
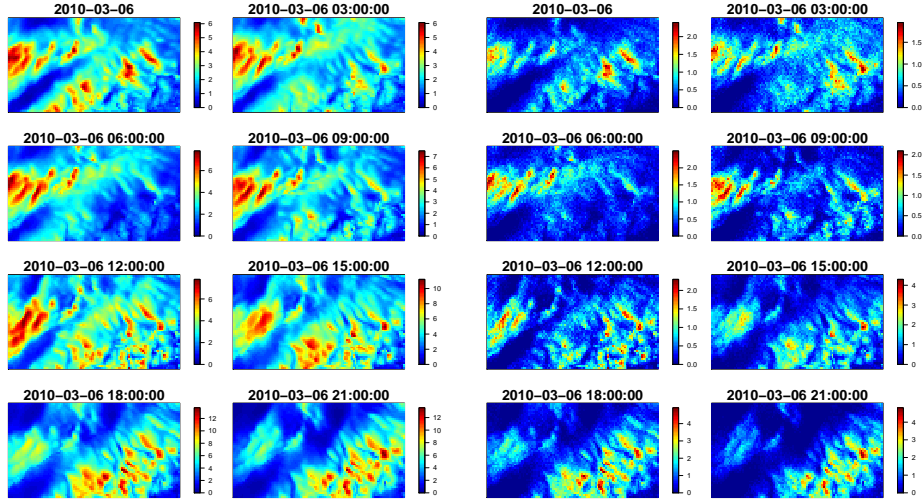


Figure 9. Comparison of predicted and observed areal averages for the period $t = 761, \dots, 768$. Shown are means of the predictive distribution ("Stat PP Mean"), 95% predictive intervals ("Stat PP Quantile"), and areal means obtained from the NWP model. All quantities are in mm.

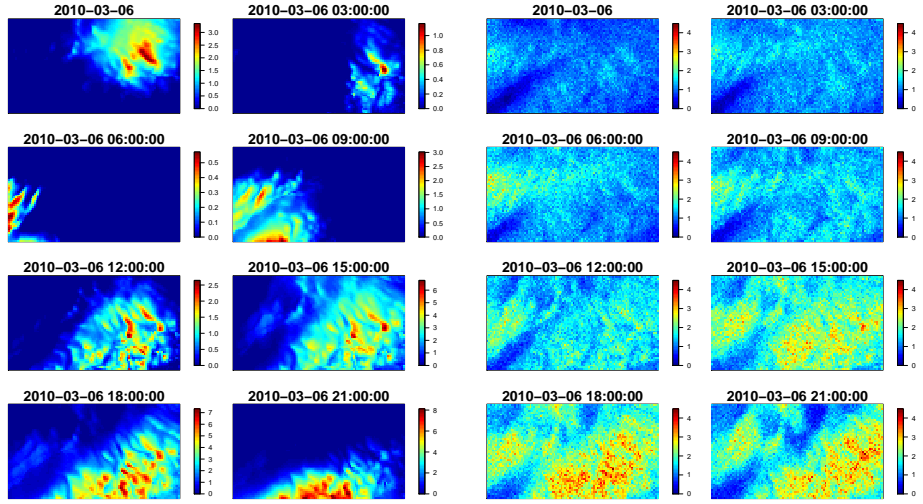
butions over the next 24 hours. Figure 9 compares postprocessed areal averages and areal averages from the NWP model with observed areal averages. Due to data availability, we restrict ourselves to the 32 stations at which observations are made. Concerning the statistically postprocessed forecasts, the mean and 95% predictive intervals are shown. In this case, the NWP model predicted too high precipitation averages. The statistically postprocessed forecasts, on the other hand, are in line with the observations. Note how the predictive distribution becomes wider with increasing lead time.

The statistical model produces a joint spatio-temporal predictive distribution that is spatially highly resolved. Depending on the specific application, several quantities of this distribution can be of interest. Some of these are illustrated in Figure 10. Predicted fields for the period $t = 761, \dots, 768$ from the NWP are shown in the top left corner. On the right of it are pointwise medians obtained from the statistical forecasts. For illustration, we also show one sample from the predictive distribution. To quantify prediction uncertainty, the difference between the third quartile and the median of the predictive distribution is plotted. These plots again show the growing uncertainty with increasing lead time. Other quantities of interest (not shown here to save space), that can be easily obtained, include probabilities of precipitation occurrence or various quantiles of the distribution.



(a) NWP

(b) Median



(c) One sample

(d) Quartile difference

Figure 10. Illustration of postprocessed spatio-temporal precipitation fields for the period $t = 761, \dots, 768$. The figure shows the NWP forecasts (a), point-wise medians of the predictive distribution (b), one sample from the predictive distribution (c), and the differences between the third quartile and the median of the predictive distribution (d). All quantities are in mm.

7 CONCLUSION

We have introduced a dynamic spatio-temporal model for large data sets. This was done by constructing a reduced dimensional approximation of an SPDE in the spectral space. We thus obtain a spatio-temporal Gaussian process that can deal with spatially and temporally highly resolved data. Its parametrization is physically motivated and allows for a nonseparable and, potentially, temporally nonstationary covariance structures. The proposed model is applied to postprocessing of precipitation forecasts for northern Switzerland. The postprocessed forecasts clearly outperform the raw NWP predictions. In addition, they have the advantage that they quantify prediction uncertainty.

Further research can be done in the following directions. Even though the intention is not to solve the SPDE as well as possible, an open topic can be a theoretical investigation on the quality of the low-dimensional spectral approximation to the solution of the SPDE. Another interesting direction for further research would be to extend the model to allow for spatial non-stationarity in the innovation field or in the autoregressive operator. Even though the computational burden has been considerably reduced by using a low rank approximation, it would be desirable to have faster methods for fitting the model.

ACKNOWLEDGMENTS

We thank Vanessa Stauch from MeteoSchweiz for providing the data and for inspiring discussions.

References

- Anderson, B. D. O. and Moore, J. B. (1979), *Optimal filtering / Brian D. O. Anderson, John B. Moore*, Prentice-Hall, Englewood Cliffs, N.J. :.
- Antolik, M. S. (2000), “An overview of the National Weather Service’s centralized statistical quantitative precipitation forecasts,” *Journal of Hydrology*, 239, 306 – 337.
- Applequist, S., Gahrs, G. E., Pfeffer, R. L., and Niu, X.-F. (2002), “Comparison of Methodologies for Probabilistic Quantitative Precipitation Forecasting,” *Weather and Forecasting*, 17, 783–799.
- Banerjee, S., Carlin, B. P., and Gelfand, A. E. (2004), *Hierarchical Modeling and Analysis for Spatial Data*, Monographs on Statistics and Applied Probability, Chapman and Hall/CRC.
- Banerjee, S., Gelfand, A. E., Finley, A. O., and Sang, H. (2008), “Gaussian predictive process models for large spatial data sets,” *Journal Of The Royal Statistical Society Series B*, 70, 825–848.
- Bardossy, A. and Plate, E. (1992), “Space-time model for daily rainfall using atmospheric circulation patterns,” *Water Resources Research*, 28, 1247–1259.

- Bell, T. (1987), “A space-time stochastic model of rainfall for satellite remote-sensing studies,” *Journal of Geophysical Research*, 92, 9631–9643.
- Berrocal, V. J., Raftery, A. E., and Gneiting, T. (2008), “Probabilistic quantitative precipitation field forecasting using a two-stage spatial model,” *Annals of Applied Statistics*, 2, 1170–1193.
- Bjørnar Bremnes, J. (2004), “Probabilistic Forecasts of Precipitation in Terms of Quantiles Using NWP Model Output,” *Monthly Weather Review*, 132, 338–347.
- Borgman, L., Taheri, M., and Hagan, R. (1984), “Three-dimensional frequency-domain simulations of geological variables,” in *Geostatistics for Natural Resources Characterization*, ed. Verly, G., D. Reidel, pp. 517–541.
- Brown, P. E., Karesen, K. F., Roberts, G. O., and Tonellato, S. (2000), “Blur-Generated Non-Separable Space-Time Models,” *Journal of the Royal Statistical Society. Series B (Statistical Methodology)*, 62, 847–860.
- Carter, C. K. and Kohn, R. (1994), “On Gibbs Sampling for State Space Models,” *Biometrika*, 81, 541–553.
- Coe, R. and Stern, R. (1982), “Fitting Models to Daily Rainfall Data,” *Journal of Applied Meteorology*, 21, 1024–1031.
- Cooley, J. W. and Tukey, J. W. (1965), “An algorithm for the machine calculation of complex Fourier series,” *Math. Comp.*, 19, 297–301.
- Cressie, N. and Huang, H.-C. (1999), “Classes of Nonseparable, Spatio-Temporal Stationary Covariance Functions,” *Journal of the American Statistical Association*, 94, 1330–1340.
- Cressie, N. and Johannesson, G. (2008), “Fixed rank kriging for very large spatial data sets,” *Journal of the Royal Statistical Society: Series B (Statistical Methodology)*, 70, 209–226.
- Duan, J. A., Gelfand, A. E., and Sirmans, C. (2009), “Modeling space-time data using stochastic differential equations,” *Bayesian Analysis*, 4, 733–758.
- Dudgeon, D. E. and Mersereau, R. M. (1984), *Multidimensional digital signal processing*, Prentice-Hall.
- Eidsvik, J., Shaby, B., Reich, B., Wheeler, M., and Niemi, J. (2011), “Estimation and prediction in spatial models with block composite likelihoods using parallel computing,” *Preprint* (<http://www.math.ntnu.no/~joeid/ESRWN.pdf>).
- Friederichs, P. and Hense, A. (2007), “Statistical Downscaling of Extreme Precipitation Events Using Censored Quantile Regression,” *Monthly Weather Review*, 135, 2365–2378.

- Frühwirth-Schnatter, S. (1994), “Data Augmentation and Dynamic Linear Models,” *Journal of Time Series Analysis*, 15, 183–202.
- Fuentes, M. (2007), “Approximate Likelihood for Large Irregularly Spaced Spatial Data,” *Journal of the American Statistical Association*, 102, 321–331.
- Furrer, R., Genton, M. G., and Nychka, D. (2006), “Covariance Tapering for Interpolation of Large Spatial Datasets,” *Journal of Computational and Graphical Statistics*, 15, 502–523.
- Gelfand, A. E., Banerjee, S., and Gamerman, D. (2005), “Spatial process modelling for univariate and multivariate dynamic spatial data,” *Environmetrics*, 16, 465–479.
- Gelfand, A. E. and Smith, A. F. M. (1990), “Sampling-Based Approaches to Calculating Marginal Densities,” *Journal of the American Statistical Association*, 85, 398–409.
- Gilks, W. R., Richardson, S., and Spiegelhalter, D. J. (1996), *Markov Chain Monte Carlo in Practice*, London: Chapman and Hall.
- Gneiting, T. (2002), “Nonseparable, Stationary Covariance Functions for Space-Time Data,” *Journal of the American Statistical Association*, 97, 590–600.
- Gneiting, T., Balabdaoui, F., and Raftery, A. E. (2007a), “Probabilistic forecasts, calibration and sharpness,” *Journal Of The Royal Statistical Society Series B*, 69, 243–268.
- Gneiting, T., Genton, M. G., and Guttorp, P. (2007b), “Geostatistical Space-Time Models, Stationarity, Separability and Full Symmetry,” in *Modelling Longitudinal and Spatially Correlated Data*, eds. Finkenstädt, B., Held, L., and Isham, V., Boca Raton: Chapman & Hall/CRC, vol. 107 of *Monographs on Statistics and Applied Probability*, pp. 151–175.
- Gneiting, T. and Raftery, A. E. (2005), “Weather Forecasting with Ensemble Methods,” *Science*, 310, 248–249.
- (2007), “Strictly Proper Scoring Rules, Prediction, and Estimation,” *Journal of the American Statistical Association*, 102, 359–378.
- Golightly, A. and Wilkinson, D. (2008), “Bayesian inference for nonlinear multivariate diffusion models observed with error,” *Computational & Statistics Data Analysis*, 52, 1674 – 1693.
- Guttorp, P. and Gneiting, T. (2006), “Studies in the history of probability and statistics XLIX On the Matrn correlation family,” *Biometrika*, 93, 989–995.
- Hamill, T. M. and Colucci, S. J. (1997), “Verification of Eta RSM Short-Range Ensemble Forecasts,” *Monthly Weather Review*, 125, 1312–1327.
- Hamill, T. M., Whitaker, J. S., and Wei, X. (2004), “Ensemble Reforecasting: Improving Medium-Range Forecast Skill Using Retrospective Forecasts,” *Monthly Weather Review*, 132, 1434–1447.

- Handcock, M. S. and Stein, M. L. (1993), “A Bayesian Analysis of Kriging,” *Technometrics*, 35, 403–410.
- Hastings, W. K. (1970), “Monte Carlo sampling methods using Markov chains and their applications,” *Biometrika*, 57, 97–109.
- Hotelling, H. (1927), “Differential Equations Subject to Error, and Population Estimates,” *Journal of the American Statistical Association*, 22, pp. 283–314.
- Huang, H.-C. and Hsu, N.-J. (2004), “Modeling transport effects on ground-level ozone using a non-stationary spacetime model,” *Environmetrics*, 15, 251–268.
- Hutchinson, M. (1995), “Stochastic space-time weather models from ground-based data,” *Agricultural and Forest Meteorology*, 73, 237–264.
- Johannesson, G., Cressie, N., and Huang, H.-C. (2007), “Dynamic multi-resolution spatial models,” *Environmental and Ecological Statistics*, 14, 5–25.
- Jones, R. and Zhang, Y. (1997), “Models for continuous stationary space-time processes,” in *Modelling Longitudinal and Spatially Correlated Data*, eds. Gregoire, T., Brillinger, D. R., Diggle, P. J., Russek-Cohen, E., Warren, W. G., and Wolfinger, R., New-York: Springer-Verlag, vol. 122 of *Lecture Notes in Statistics*, pp. 289–298.
- Kleiber, W., Raftery, A. E., and Gneiting, T. (2011), “Geostatistical Model Averaging for Locally Calibrated Probabilistic Quantitative Precipitation Forecasting,” *Journal of the American Statistical Association*, 106, 1291–1303.
- Krzysztofowicz, R. and Maranzano, C. J. (2006), “Bayesian Processor of Output for Probabilistic Quantitative Precipitation Forecasting,” *Working paper, Department of Systems Engineering and Department of Statistics, University Virginia*.
- Lindgren, F., Rue, H., and Lindstrom, J. (2011), “An explicit link between Gaussian fields and Gaussian Markov random fields: the stochastic partial differential equation approach,” *Journal of the Royal Statistical Society: Series B (Statistical Methodology)*, 73, 423–498.
- Ma, C. (2003), “Families of spatio-temporal stationary covariance models,” *Journal of Statistical Planning and Inference*, 116, 489 – 501.
- Malmberg, A., Arellano, A., Edwards, D. P., Flyer, N., Nychka, D., and Wikle, C. (2008), “Interpolating fields of carbon monoxide data using a hybrid statistical-physical model,” *The Annals of Applied Statistics*, 2, 1231–1248.
- Matheson, J. E. and Winkler, R. L. (1976), “Scoring Rules for Continuous Probability Distributions,” *Management Science*, 22, pp. 1087–1096.
- Metropolis, N., Rosenbluth, A. W., Rosenbluth, M. N., Teller, A. H., and Teller, E. (1953), “Equation of State Calculations by Fast Computing Machines,” *The Journal of Chemical Physics*, 21, 1087–1092.

- Neal, P. and Roberts, G. (2006), “Optimal Scaling for Partially Updating MCMC Algorithms,” *The Annals of Applied Probability*, 16, pp. 475–515.
- Nychka, D., Wikle, C., and Royle, J. A. (2002), “Multiresolution models for nonstationary spatial covariance functions,” *Statistical Modeling*, 2, 315–331.
- Paciorek, C. J. (2007), “Bayesian Smoothing with Gaussian Processes Using Fourier Basis Functions in the spectralGP Package,” *Journal of Statistical Software*, 19.
- Paciorek, C. J. and Schervish, M. J. (2006), “Spatial modelling using a new class of nonstationary covariance functions,” *Environmetrics*, 17, 483–506.
- Palmer, T. N. (2002), “The economic value of ensemble forecasts as a tool for risk assessment: From days to decades,” *Quarterly Journal of the Royal Meteorological Society*, 128, 747–774.
- Ramrez, M. C. V., de Campos Velho, H. F., and Ferreira, N. J. (2005), “Artificial neural network technique for rainfall forecasting applied to the So Paulo region,” *Journal of Hydrology*, 301, 146 – 162.
- Robert, C. P. and Casella, G. (2004), *Monte Carlo Statistical Methods, Second Edition*, Springer Texts in Statistics, Spring Street, New York, NY 10013, USA: Springer Science and Business Media Inc., 2nd ed.
- Roberts, G. O. and Rosenthal, J. S. (2001), “Optimal Scaling for Various Metropolis-Hastings Algorithms,” *Statistical Science*, 16, pp. 351–367.
- (2009), “Examples of Adaptive MCMC,” *Journal of Computational and Graphical Statistics*, 18, 349–367.
- Roberts, G. O. and Stramer, O. (2001), “On Inference for Partially Observed Nonlinear Diffusion Models Using the Metropolis-Hastings Algorithm,” *Biometrika*, 88, pp. 603–621.
- Royle, J. A. and Wikle, C. K. (2005), “Efficient statistical mapping of avian count data,” *Environmental and Ecological Statistics*, 12, 225–243.
- Rue, H. and Held, L. (2005), *Gaussian Markov random fields*, vol. 104 of *Mono-graphs on Statistics and Applied Probability*, Chapman & Hall/CRC, Boca Raton, FL, theory and applications.
- Rue, H., Martino, S., and Chopin, N. (2009), “Approximate Bayesian inference for latent Gaussian models by using integrated nested Laplace approximations,” *Journal Of The Royal Statistical Society Series B*, 71, 319–392.
- Rue, H. and Tjelmeland, H. (2002), “Fitting Gaussian Markov Random Fields to Gaussian Fields,” *Scandinavian Journal of Statistics*, 29, 31–49.
- Sanso, B. and Guenni, L. (2004), “A Bayesian approach to compare observed rainfall data to deterministic simulations,” *Environmetrics*, 15, 597–612.

- Shumway, R. H. and Stoffer, D. S. (2000), *Time series analysis and its applications*, Springer Texts in Statistics, New York: Springer-Verlag.
- Sigrist, F., Kuensch, H. R., and Stahel, W. A. (2012), “A Dynamic Non-stationary Spatio-temporal Model for Short Term Prediction of Precipitation,” *Preprint* (<http://arxiv.org/abs/1102.4210>).
- Sloughter, J. M., Raftery, A. E., Gneiting, T., and Fraley, C. (2007), “Probabilistic quantitative precipitation forecasting using Bayesian model averaging,” *Monthly Weather Review*, 135, 3209–3220.
- Solna, K. and Switzer, P. (1996), “Time Trend Estimation for a Geographic Region,” *Journal of the American Statistical Association*, 91, 577–589.
- Stein, M. L. (2005), “Space-Time Covariance Functions,” *Journal of the American Statistical Association*, 100, 310–321.
- (2008), “A modeling approach for large spatial datasets,” *Journal of the Korean Statistical Society*, 37, 3 – 10.
- Stein, M. L., Chi, Z., and Welty, L. J. (2004), “Approximating likelihoods for large spatial data sets,” *Journal of the Royal Statistical Society: Series B (Statistical Methodology)*, 66, 275–296.
- Stensrud, D. J. and Yussouf, N. (2007), “Reliable Probabilistic Quantitative Precipitation Forecasts from a Short-Range Ensemble Forecasting System,” *Weather and Forecasting*, 22, 2–17.
- Steppeler, J., Doms, G., Schttler, U., Bitzer, H. W., Gassmann, A., Damrath, U., and Gregoric, G. (2003), “Meso-gamma scale forecasts using the nonhydrostatic model LM,” *Meteorology and Atmospheric Physics*, 82, 75–96.
- Stidd, C. K. (1973), “Estimating the Precipitation Climate,” *Water Resources Research*, 9, 1235–1241.
- Storvik, G., Frigessi, A., and Hirst, D. (2002), “Stationary space-time Gaussian fields and their time autoregressive representation,” *Stat. Model.*, 2, 139–161.
- Stroud, J. R., Stein, M. L., Lesht, B. M., Schwab, D. J., and Beletsky, D. (2010), “An Ensemble Kalman Filter and Smoother for Satellite Data Assimilation,” *Journal of the American Statistical Association*, 105, 978–990.
- Sun, Y., Li, B., and Genton, M. G. (2012), “Geostatistics for Large Datasets,” in *Advances and Challenges in Space-time Modelling of Natural Events*, eds. Porcu, E., Montero, J., and Schlather, M., Springer-Verlag, vol. 207 of *Lecture Notes in Statistics*, pp. 55–77.
- Tobin, J. (1958), “Estimation of relationships for limited dependent variables,” *Econometrica*, 26, 24–36.
- Vecchia, A. V. (1988), “Estimation and Model Identification for Continuous Spatial Processes,” *Journal of the Royal Statistical Society. Series B (Methodological)*, 50, pp. 297–312.

- Vivar, J. C. and Ferreira, M. A. R. (2009), “Spatiotemporal Models for Gaussian Areal Data,” *Journal of Computational and Graphical Statistics*, 18, 658–674.
- Whittle, P. (1954), “On Stationary Processes in the Plane,” *Biometrika*, 41, pp. 434–449.
- Wikle, C. and Hooten, M. (2010), “A general science-based framework for dynamical spatio-temporal models,” *TEST*, 19, 417–451.
- Wikle, C. K. (2003), “Hierarchical Bayesian Models for Predicting the Spread of Ecological Processes,” *Ecology*, 84, pp. 1382–1394.
- Wikle, C. K., Berliner, L. M., and Cressie, N. (1998), “Hierarchical Bayesian space-time models,” *Environmental and Ecological Statistics*, 5, 117–154.
- Wikle, C. K. and Cressie, N. (1999), “A Dimension-Reduced Approach to Space-Time Kalman Filtering,” *Biometrika*, 86, 815–829.
- Wilks, D. (1990), “Maximum likelihood estimation for the gamma distribution using data containing zeros,” *Journal of Climate*, 3, 1495–1501.
- (1999), “Multisite downscaling of daily precipitation with a stochastic weather generator,” *Climate Research*, 11, 125–136.
- Woodbury, M. A. (1950), *Inverting modified matrices*, Statistical Research Group, Memo. Rep. no. 42, Princeton University, Princeton, N. J.
- Xu, K. and Wikle, C. K. (2007), “Estimation of parameterized spatio-temporal dynamic models,” *Journal of Statistical Planning and Inference*, 137, 567 – 588.
- Xu, K., Wikle, C. K., and Fox, N. I. (2005), “A Kernel-Based Spatio-Temporal Dynamical Model for Nowcasting Weather Radar Reflectivities,” *Journal of the American Statistical Association*, 100, 1133–1144.
- Yussouf, N. and Stensrud, D. J. (2006), “Prediction of Near-Surface Variables at Independent Locations from a Bias-Corrected Ensemble Forecasting System,” *Monthly Weather Review*, 134, 3415–3424.
- Zheng, Y. and Aukema, B. H. (2010), “Hierarchical dynamic modeling of outbreaks of mountain pine beetle using partial differential equations,” *Environmetrics*, 21, 801–816.